

# Optimal sampling of dynamical large deviations in two dimensions via tensor networks

Luke Causer,<sup>1,2</sup> Mari Carmen Bañuls,<sup>3,4</sup> and Juan P. Garrahan<sup>1,2</sup>

<sup>1</sup>*School of Physics and Astronomy, University of Nottingham, Nottingham, NG7 2RD, UK*

<sup>2</sup>*Centre for the Mathematics and Theoretical Physics of Quantum Non-Equilibrium Systems, University of Nottingham, Nottingham, NG7 2RD, UK*

<sup>3</sup>*Max-Planck-Institut für Quantenoptik, Hans-Kopfermann-Str. 1, D-85748 Garching, Germany*

<sup>4</sup>*Munich Center for Quantum Science and Technology (MCQST), Schellingstr. 4, D-80799 München*

We use projected entangled-pair states (PEPS) to calculate the large deviations (LD) statistics of the dynamical activity of the two dimensional East model, and the two dimensional symmetric simple exclusion process (SSEP) with open boundaries, in lattices of up to  $40 \times 40$  sites. We show that at long-times both models have phase transitions between active and inactive dynamical phases. For the 2D East model we find that this trajectory transition is of the first-order, while for the SSEP we find indications of a second order transition. We then show how the PEPS can be used to implement a trajectory sampling scheme capable of directly accessing rare trajectories. We also discuss how the methods described here can be extended to study rare events at finite times.

**Introduction.-** Over the last few years we have seen progress in the application of numerical tensor network (TN) techniques to compute statistical properties of dynamical trajectories in classical stochastic systems. The first such application was to long time statistics—the dynamical large deviation (LD) regime—of one-dimensional lattice systems using variational algorithms (such as density matrix renormalization group [1], or DMRG) to approximate the leading eigenvectors of tilted Markov generators by matrix product states (MPS, e.g. Ref. [2]) [3–10]. Building on these results, we introduced a sampling method which exploited such MPS to efficiently sample rare trajectories, and then presented a method based on MPS time-evolution to precisely compute trajectory statistics at finite times [11]. For more than one spatial dimension, a more suitable variational class is that of projected-entangled pair states (PEPS) [12], which fulfills an entanglement area law [13] and was recently applied to the classical asymmetric exclusion process in two dimensions in Ref. [14]. A computationally cheaper alternative, without an area law, but accommodating more entanglement than MPS, is that of tree tensor networks (TTN) [15], used for example in Refs. [16, 17], in combination with a time-dependent variational principle [18] to study driven problems.

Here we use PEPS to study the large deviations of the *dynamical activity* in two paradigmatic two-dimensional models, the 2D East model (also known as North-or-East model) [19–22], and the 2D symmetric simple exclusion process (SSEP) with open boundaries where particles can be injected and removed [23]. We are able to accurately estimate the leading eigenvector of the tilted generator, and thus the LDs, of these models using the *simple update* (SU) algorithm for PEPS, see e.g. [24], and verify that further improvements can come from more complex update schemes, such as *full update* (FU), see e.g. [25, 26]. We then use the approximate leading eigenvector to construct an auxiliary dynamics which can directly sample the corresponding rare trajectories. Such an algorithm

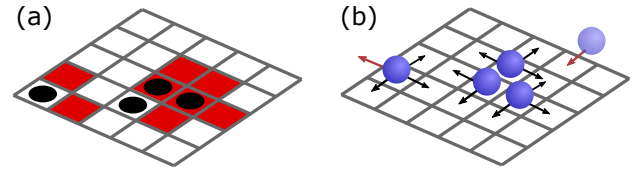


FIG. 1. **Models.** (a) The 2D East model. An occupation, shown by the black circles, can facilitate flips marked by the red-coloured cells at the neighbouring sites, but only in two directions. (b) The 2D SSEP. The sites on the lattice can be occupied by particles which can hop in any direction, as long as the target site is not occupied. Particles can enter or leave at the boundaries, as shown by the red arrows.

requires efficient sampling from the PEPS, and we show how to do this in the context of trajectory sampling. We benchmark our methods, showing how the bond dimension of the PEPS allows for a controlled accuracy of optimal dynamics. We demonstrate that both models have a phase transition between active and inactive dynamical phases, a first-order transition for the 2D East and a second-order transition for the 2D SSEP.

**Models.-** The models we study here live in a two-dimensional square lattice of size  $N = L \times L$ , with each site being occupied by a binary variable  $n_{\mathbf{k}} = 0$  or  $1$ , where  $\mathbf{k} = (k_x, k_y)$  denotes the position of the site for  $k_x, k_y = 1 \dots L$ . Their continuous-time dynamics is defined by a Markov generator (e.g. see Refs. [27, 28]),

$$\mathbb{W} = \sum_{x,y \neq x} w_{x \rightarrow y} |y\rangle \langle x| - \sum_x R_x |x\rangle \langle x|, \quad (1)$$

where  $|x\rangle$  and  $|y\rangle$  are configurations on the lattice,  $w_{x \rightarrow y}$  the transition rate from  $x$  to  $y$ , and  $R_x = \sum_{y \neq x} w_{x \rightarrow y}$  the escape rate out of  $x$ . We can write this as  $\mathbb{W} = \mathbb{K} - \mathbb{R}$ , where  $\mathbb{K}$  contains the off-diagonal transition rates, and  $\mathbb{R}$  the diagonal escape rates.

The first model we consider is the 2D East model [19–22], often studied in the context of the glass transition.

This is a kinetically constrained model (KCM) such that an excited site  $n_{\mathbf{k}} = 1$ , allows (“facilitates”) a site to its North or East to flip stochastically, see Fig. 1(a). The generator of the 2D East model reads

$$\mathbb{W}^{\text{East}} = \sum_{\mathbf{k}} P_{\mathbf{k}} \left[ c (\sigma_{\mathbf{k}}^+ - (1 - n_{\mathbf{k}})) + (1 - c) (\sigma_{\mathbf{k}}^- - n_{\mathbf{k}}) \right], \quad (2)$$

where  $c \in (0, 1/2]$  controls the average occupation density, and the kinetic constraint is  $P_{(k_x, k_y)} = n_{(k_x-1, k_y)} + n_{(k_x, k_y-1)}$ . In addition, we choose open boundary conditions (OBC) with  $n_{(1,1)} = 1$  fixed. This ensures the entire state space remains dynamically connected [20].

The second model is the 2D SSEP. This describes particles hopping to neighbouring sites on a 2D lattice with unit rate, but only if the target site is not already occupied by a particle. We also allow particles to be injected or removed at the boundaries of the lattice with rate  $1/2$ , see Fig. 1(b). The generator for the SSEP is

$$\mathbb{W}_{\text{SSEP}} = \sum_{\langle \mathbf{k}, \mathbf{l} \rangle} \left[ \sigma_{\mathbf{k}}^+ \sigma_{\mathbf{l}}^- - (1 - n_{\mathbf{k}}) n_{\mathbf{l}} + \sigma_{\mathbf{k}}^- \sigma_{\mathbf{l}}^+ - n_{\mathbf{k}} (1 - n_{\mathbf{l}}) \right] + \frac{1}{2} \sum_{\mathbf{k} \in \partial} \left[ \sigma_{\mathbf{k}}^x - 1 \right], \quad (3)$$

where  $\langle \mathbf{k}, \mathbf{l} \rangle$  denotes a pair of nearest neighbours, and  $\partial$  the boundary of the lattice.

**Dynamical LDs.-** We consider the statistics of some dynamical observable  $\hat{K}$  through its probability distribution  $P_t(K) = \sum_{\omega_t} \pi(\omega_t) \delta[\hat{K}(\omega_t) - K]$ , where  $\omega_t$  denotes a stochastic trajectory and  $\pi(\omega_t)$  is the probability it occurs under the stochastic generator  $\mathbb{W}$ . Essentially the same information is encoded in the moment generating function (MGF),  $Z_t(s) = \sum_{\omega_t} \pi(\omega_t) e^{-s\hat{K}(\omega_t)}$ , where we have introduced the counting field  $s$ . In the  $t \rightarrow \infty$  limit, the two obey LD principles  $P_t(K) \asymp e^{-t\varphi(K/t)}$  and  $Z_t(s) \asymp e^{t\theta(s)}$ , with the rate function  $\varphi(K/t)$  and scaled cumulant generating function (SCGF)  $\theta(s)$  being time-independent. The LD functions are related through a Legendre transform,  $\varphi(k) = -\min_s [\theta(s) + sk(s)]$ , for  $k = K/t$ . For reviews, see Refs. [28–31].

A convenient way to determine the SCGF is to construct a biased or *tilted* generator [29, 32–34], a (non-stochastic) deformation of the Markov generator  $\mathbb{W}$  such that the associated trajectories are exponentially biased by  $e^{-s\hat{K}(\omega_t)}$ . We consider as an observable the *dynamical activity* [32, 35], which counts the number of jumps in a stochastic trajectory and thus quantifies the overall level of motion. The corresponding tilted generator then takes the form  $\mathbb{W}_s = e^{-s\mathbb{K}} - \mathbb{R}$ . The SCGF can be retrieved by calculating the largest eigenvalue and eigenvector(s),

$$\mathbb{W}_s |r_s\rangle = \theta(s) |r_s\rangle, \quad \langle l_s | \mathbb{W}_s = \theta(s) \langle l_s|. \quad (4)$$

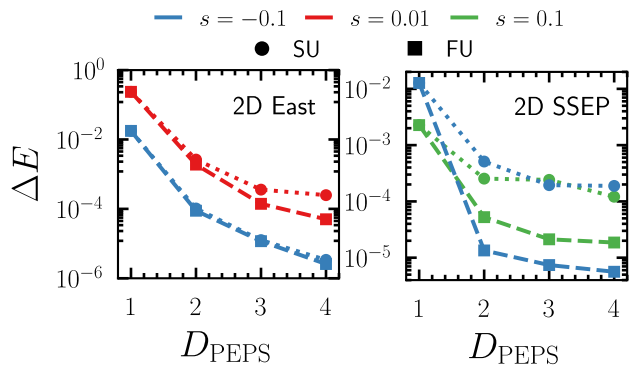


FIG. 2. **Optimization of PEPS.** The error in measured energy for the SU and the FU compared to the high accuracy 2D DMRG (with a MPS bond dimension up to  $D_{\text{MPS}} = 1024$ ) for various values of  $s$  and a  $10 \times 10$  lattice. The left panel shows the 2D East model with  $c = 0.5$ , and the right panel shows the 2D SSEP. The PEPS environment in the FU uses a boundary dimension  $\chi_B = 4D^2$  for the East and  $\chi_B = 6D^2$  for the SSEP.

For the models and dynamical observable considered here, we can introduce a similarity transformation independent of  $s$ ,  $\mathbb{H}_s = -\mathbb{P}^{-1} \mathbb{W}_s \mathbb{P}$ , where  $\mathbb{P}$  is a diagonal matrix with the square roots of the steady state probabilities [34]. This results in a Hermitian matrix with minimal eigenvalue and associated eigenvector

$$\mathbb{H}_s |\psi_s\rangle = -\theta(s) |\psi_s\rangle, \quad (5)$$

where  $|\psi_s\rangle$  is related to the original eigenvectors by  $|r_s\rangle = \mathbb{P} |\psi_s\rangle$  and  $\langle l_s | = \langle \psi_s | \mathbb{P}^{-1}$ . This representation is convenient as the minimum eigenvalue is bounded by the Rayleigh-Ritz principle.

**PEPS.-** Determining the minimal eigenvalue and eigenvector of  $\mathbb{H}_s$  boils down to an optimization problem. We approach this using TN methods. A natural ansatz choice in this case is PEPS, the direct two-dimensional generalization of MPS [12]. PEPS are known to obey the area law in 2D [36], with the amount of entanglement controlled by its virtual bond dimension  $D_{\text{PEPS}}$ . To calculate observables we also need a scheme to contract the TN. For the case of PEPS, this cannot be done efficiently and thus we have to use an approximate scheme. We use the boundary MPS scheme [12, 37], where we contract from the edge of a PEPS network with an MPS with some boundary dimension  $\chi_B$  which controls the accuracy of contraction. A common heuristic choice for local problems is  $\chi_B \sim O(D_{\text{PEPS}}^2)$  (see e.g. Ref. [38]).

The final step is to choose an update scheme to estimate the wavefunction  $|\psi_s\rangle$ . Broadly speaking, there are three popular approaches. The computationally cheapest but least precise is the SU scheme [24], which we use for the most part here. SU makes use of imaginary time evolution, with updates which only consider the local environment. It is not optimal but only entails compu-

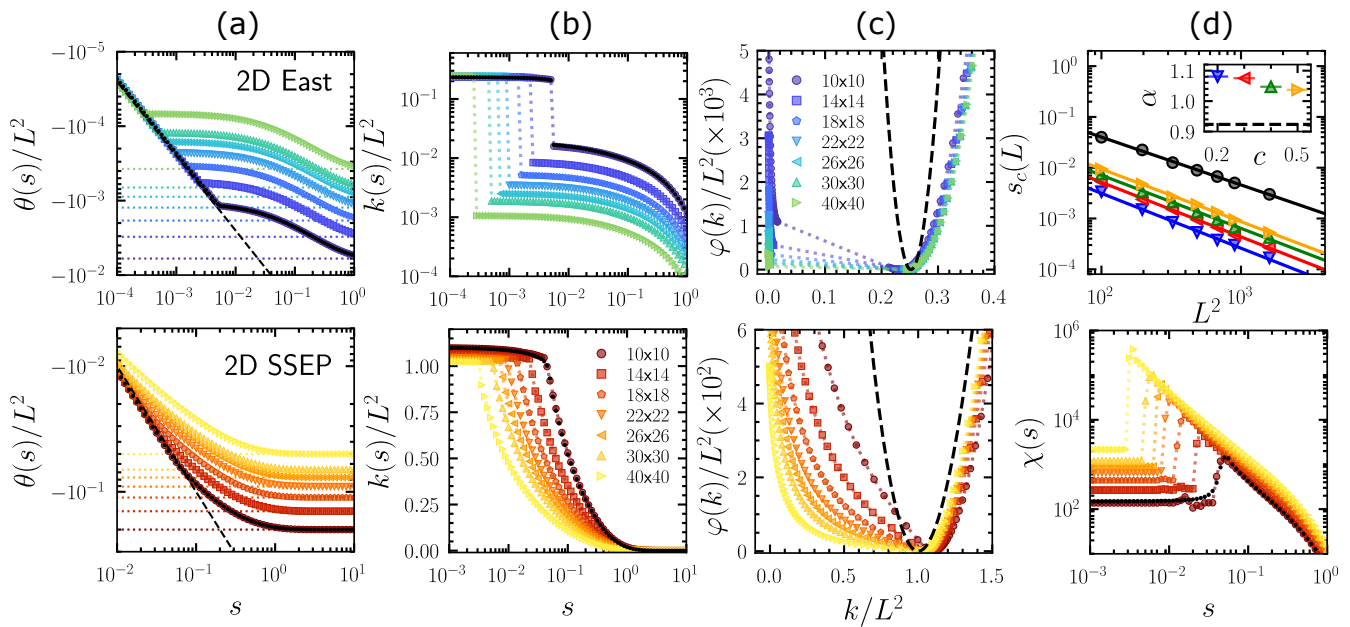


FIG. 3. **Dynamical large deviations and active-inactive transitions from PEPS.** (a) The SCGF  $\theta(s)/L^2$  for the 2D East with  $c = 0.3$  (top) and the SSEP (bottom) for system sizes  $N \in [10^2, 40^2]$ . The black dashed line shows the linear response for small  $s$ , and the colour dotted lines show the value for  $s \rightarrow \infty$ . (b) The dynamical activity  $k(s)/L^2$  for the systems in (a). The East is on a log-log scale, and the SSEP a log-linear scale. (c) The rate function  $\varphi(k)/L^2$  as a function of activity  $k/L^2$  for the systems in (a). The dashed line shows the Poisson distribution with mean  $k(s=0)/L^2$ . (d) The transition points  $s_c(L)$  for the 2D SSEP (black circles) and the 2D East for  $c \in [0.2, 0.5]$ . The solid lines show the fitted power-law curves  $s_c(L) \sim L^{-2\alpha}$ , with the exponents shown in the inset. The black dashed line is the exponent for the SSEP, and the symbols are for the East. The symbols can be used to read the value of  $c$  in the main figure. The bottom panel shows the dynamical susceptibility  $\chi(s) = \theta''(s)$  for the 2D SSEP. All the data was acquired using the SU except for the black markers, which show 2D DMRG data for a  $N = 10$  lattice for comparison.

tation cost of  $O(D_{\text{PEPS}}^5)$  [39]. A more efficient update which also relies on imaginary time evolution is the FU [25, 26]: here we have to contract the whole TN (except for the tensors which are being updated). While this costs  $O(\chi_B^3 D_{\text{PEPS}}^4 + \chi_B^2 D_{\text{PEPS}}^6)$ , with a good approximate environment it ensures the update is optimal. The final class of updates are Variational Updates (VU) [40, 41] which we do not consider here. For details see e.g. Ref. [42].

Figure 2 compares the SU and FU schemes [43] for both models against 2D DMRG [44] for small  $10 \times 10$  lattices, where almost exact results can be determined with DMRG [45]. We show the relative difference in energy  $\Delta E = (E_{\text{PEPS}} - E_{\text{DMRG}})/E_{\text{DMRG}}$ . We find that the SU is able to achieve accuracy  $\delta E < 10^{-3}$ , which is enough for our study. Even though the FU could improve the results, we thus proceed with SU with a maximal bond dimension  $D_{\text{PEPS}} = 4$ , which allows us reaching large sizes at low computational cost.

**Large deviations from PEPS.**— The East and SSEP in 1D are known to have LD transitions in terms of the activity or other dynamical observables [6, 8, 32, 46–52]. In two-dimensions, the SSEP has a transition in the LDs of the current [14]. We now provide evidence

by means of PEPS for both the 2D East and 2D SSEP having active-inactive phase transitions. Figure 3(a-c) shows the LD statistics for both the 2D East model (top) and the 2D SSEP (bottom). For the East model, we see from Fig. 3(a) that the SCGF follows linear response,  $\theta(s) \approx sk(0)$ , for small  $s$ , but at  $s_c(L)$  it sharply changes to another branch. This point corresponds to a sudden drop in activity,  $k(s) = -\theta'(s)$ , which becomes discontinuous in the limit  $N \rightarrow \infty$ , see Fig. 3(b). Having access to both the SCGF and the dynamical activity allows us to estimate the rate function  $\varphi(k)$ , shown in Fig. 3(c). We see broadening of the rate function around the mean, indicating the coexistence of active and inactive dynamics. All this behaviour is characteristic of a first-order phase transition.

For the SSEP we see something different: Fig. 3(a) shows no sharp change in  $\theta(s)$ , and the activity in Fig. 3(b) has no discontinuity. This is indicative of a second-order transition, with the rate function showing critical broadening, see Fig. 3(c), and a divergence in the susceptibility  $\chi(s) = \theta''(s)$ , see Fig. 3(d). Note that this is different from the 1D SSEP with open boundaries [8] in which this transition is first-order.

For both models we can extract a transition point from

the drop in either first or second cumulant. The top panel of Fig. 3(d) shows how the transition point scales with  $L$  for both models (for a range of  $c$  for the 2D East). We are able to fit the data with the power laws  $s_c(L) \sim L^{-2\alpha}$ , as shown by the solid lines. We find the exponents  $\alpha \gtrsim 1$  for the 2D East and  $\alpha \lesssim 1$  for the SSEP, see inset to the top panel of Fig. 3(d).

**Optimal sampling of rare trajectories from PEPS.-** Sampling trajectories corresponding to the  $s \neq 0$  phases is difficult as they are exponentially rare in system size and time. The optimal sampling dynamics at long times is given by the so-called *generalized Doob transform* [53–57], which maps the tilted generator into a true stochastic generator for the rare trajectories,  $\mathbb{W}_s^{\text{Doob}} = \mathbb{L}[\mathbb{W}_s - \theta(s)\mathbb{I}]\mathbb{L}^{-1}$ , where  $\mathbb{L}$  is the leading left eigenvector of  $\mathbb{W}_s$  as a diagonal matrix. This gives a new dynamics with the transition rates

$$\tilde{w}_{x \rightarrow y} = \frac{l_s(y)}{l_s(x)} e^{-s} w_{x \rightarrow y}, \quad (6)$$

with  $l_s(x) = \langle l_s | x \rangle$ . In  $\mathbb{W}_s^{\text{Doob}}$  the counting field  $s$  appears as a physical control parameter, and running dynamics with rates (6) gives trajectories at  $s \neq 0$  on demand. While optimal,  $\mathbb{W}_s^{\text{Doob}}$  is difficult to construct in general as one needs the exact left leading eigenvector. However, we can exploit our PEPS approximation to estimate the rates Eq. (6), similar to Ref. [58] for 1D and MPS.

To obtain Eq. (6) for the transitions out of a state  $x$  we calculate  $l_s(y)$  from the PEPS using a boundary dimension  $\chi_B = D_{\text{PEPS}}$  [41, 59–61], thus entailing a maximum cost  $O(ND_{\text{PEPS}}^6)$ . If we neglect the time edges of trajectories, we can estimate an time-extensive observable by importance sampling

$$\langle O \rangle_s \approx \frac{\sum_{\alpha_t} O(\alpha_t) g(\alpha_t)}{\sum_{\alpha_t} g(\alpha_t)}, \quad (7)$$

where  $\alpha_t$  denotes a trajectory generated with (6) (the *reference dynamics*), and  $O(\alpha_t)$  is the trajectory observable. The re-weighting factor  $g(\alpha_t)$  is

$$g(\omega_t) = e^{-\int_0^t dt' R(t') - \tilde{R}(t')}, \quad (8)$$

where  $R(t')$  and  $\tilde{R}(t')$  are the escape rates of the system at time  $t'$  in the original dynamics and the approximate Doob dynamics, respectively. Notice that with a large enough number of trajectories, Eq. (7) can be used to correct on the imperfections in the reference dynamics due to an imperfect PEPS approximation.

Figures 4 show results from our sampling algorithm for the 2D East with  $c = 0.5$  and the 2D SSEP, both for system sizes  $N = 22 \times 22$ . The average dynamical activity measured in trajectories (symbols) [with umbrella sampling (7,8)] coincides with that obtained directly from the PEPS (solid line), except for  $D_{\text{PEPS}} = 1$  for the East model. The accuracy of our dynamics is quantified by the

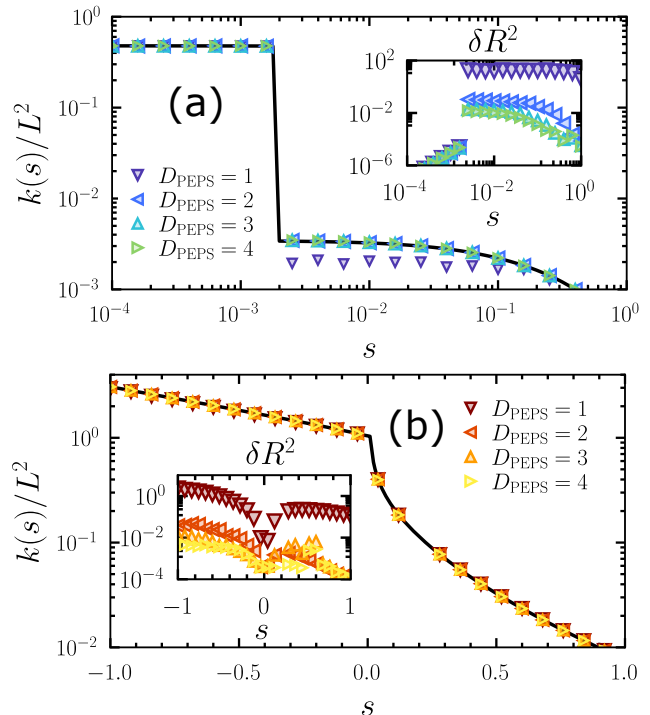


**FIG. 4. Optimal sampling of trajectories.** The average dynamical activity from CTMC with importance sampling (symbols) for the (a) 2D East model with  $c = 0.5$  and (b) the 2D SSEP respectively on a  $22 \times 22$  lattice. We show data over a range of  $s$ , and  $D_{\text{PEPS}} \in [1, 4]$ . The trajectory times are chosen such that on average we expect 100 transitions per trajectory. The solid black line shows the activity measured directly from the PEPS with  $D = 4$  for comparison. The insets show the variance in the time-integrated difference of escape rates,  $\delta R^2$  (see main text). For the East model, we show results over the dynamical phase transition  $s > 0$ , while the SSEP shows results for over negative and positive  $s$ . Each data point is calculated from  $N_{\text{sp}} \in [10^3, 10^4]$  trajectories. For visualisations of representative trajectories see Ref. [62].

variance of the time integrated difference in escape rates, cf. Eq. (8), which vanishes for the exact Doob rates. We show this for each  $D$  in the insets of Figs. 4: increasing the  $D_{\text{PEPS}}$  consistently reduces the variance, indicating a better sampling dynamics and less need for importance sampling.

**Conclusions.-** We have shown that the dynamical large deviations of two-dimensional stochastic models can be studied efficiently with PEPS, including the quasi-optimal sampling of rare trajectories. We showed here that both the 2D East model and the 2D SSEP have active-inactive trajectory transitions, of the first-order and second-order, respectively, the latter in contrast to the case of the 1D SSEP. Our work adds to the continuously expanding application [3–11, 14, 16, 17, 63] of tensor network methods to study the dynamical fluctuations in classical stochastic systems.

There are several interesting avenues to pursue building on this work. One is to integrate 2D trajectory sampling via tensor networks with a method such as transition path sampling (TPS) [64] for investigating statistics of fluctuations at *finite times*, cf. [11, 65]. While the current implementations with PEPS are too demanding to reasonably incorporate TPS, tree tensor networks (TTNs) [15] are a promising alternative that could allow to reliably investigate finite time scaling. We hope to report on this in the near future.

**Acknowledgements.-** We acknowledge financial support from EPSRC Grant no. EP/R04421X/1 and the Leverhulme Trust Grant No. RPG-2018-181. M.C.B. acknowledges support from Deutsche Forschungsgemeinschaft (DFG, German Research Foundation) under Germany’s Excellence Strategy – EXC-2111 – 390814868. Calculations were performed using the Sulis Tier 2 HPC platform hosted by the Scientific Computing Research Technology Platform at the University of Warwick. Sulis is funded by EPSRC Grant EP/T022108/1 and the HPC Midlands+ consortium. We acknowledge access to the University of Nottingham Augusta HPC service. Example code used to generate the data can be found at <https://github.com/lcauser/2d-optimal-sampling>. Data is available at from Ref. [62].

- 
- [1] S. R. White, *Phys. Rev. Lett.* **69**, 2863 (1992).  
 [2] U. Schollwöck, *Ann. Phys.* **326**, 96 (2011).  
 [3] M. Gorissen, J. Hooyberghs, and C. Vanderzande, *Phys. Rev. E* **79**, 020101 (2009).  
 [4] M. Gorissen and C. Vanderzande, *Phys. Rev. E* **86**, 051114 (2012).  
 [5] M. Gorissen, A. Lazarescu, K. Mallick, and C. Vanderzande, *Phys. Rev. Lett.* **109**, 170601 (2012).  
 [6] M. C. Bañuls and J. P. Garrahan, *Phys. Rev. Lett.* **123**, 200601 (2019).  
 [7] P. Helms, U. Ray, and G. K.-L. Chan, *Phys. Rev. E* **100**, 022101 (2019).  
 [8] L. Causer, I. Lesanovsky, M. C. Bañuls, and J. P. Garrahan, *Phys. Rev. E* **102**, 052132 (2020).  
 [9] L. Causer, J. P. Garrahan, and A. Lamacraft, *Phys. Rev. E* **106**, 014128 (2022).  
 [10] J. Gu and F. Zhang, (2022), [arXiv:2206.05322](https://arxiv.org/abs/2206.05322).  
 [11] L. Causer, M. C. Bañuls, and J. P. Garrahan, *Phys. Rev. Lett.* **128**, 090605 (2022).  
 [12] F. Verstraete and J. I. Cirac, (2004), [arXiv:cond-mat/0407066](https://arxiv.org/abs/cond-mat/0407066).  
 [13] J. Eisert, M. Cramer, and M. B. Plenio, *Rev. Mod. Phys.* **82**, 277 (2010).  
 [14] P. Helms and G. K.-L. Chan, *Phys. Rev. Lett.* **125**, 140601 (2020).  
 [15] Y.-Y. Shi, L.-M. Duan, and G. Vidal, *Phys. Rev. A* **74**, 022320 (2006).  
 [16] N. E. Strand, H. Vroylandt, and T. R. Gingrich, *J. Chem. Phys.* **156**, 221103 (2022).  
 [17] N. E. Strand, H. Vroylandt, and T. R. Gingrich, (2022), [arXiv:2201.04107](https://arxiv.org/abs/2201.04107).  
 [18] D. Bauernfeind and M. Aichhorn, *SciPost Phys.* **8**, 024 (2020).  
 [19] J. Jäckle and S. Eisinger, *Z. Phys. B* **84**, 115 (1991).  
 [20] F. Ritort and P. Sollich, *Adv. Phys.* **52**, 219 (2003).  
 [21] L. Berthier and J. Garrahan, *J. Phys. Chem. B* **109**, 3578 (2005).  
 [22] C. Casert, T. Vieijra, S. Whitelam, and I. Tambllyn, *Phys. Rev. Lett.* **127**, 120602 (2021).  
 [23] K. Mallick, *Physica A* **418**, 17 (2015).  
 [24] H. C. Jiang, Z. Y. Weng, and T. Xiang, *Phys. Rev. Lett.* **101**, 090603 (2008).  
 [25] P. Corboz, R. Orús, B. Bauer, and G. Vidal, *Phys. Rev. B* **81**, 165104 (2010).  
 [26] H. N. Phien, J. A. Bengua, H. D. Tuan, P. Corboz, and R. Orús, *Phys. Rev. B* **92**, 035142 (2015).  
 [27] C. Gardiner, *Handbook of stochastic methods* (Berlin: Springer, 2004).  
 [28] J. P. Garrahan, *Physica A* **504**, 130 (2018).  
 [29] H. Touchette, *Phys. Rep.* **478**, 1 (2009).  
 [30] H. Touchette, *Physica A* **504**, 5 (2018).  
 [31] R. L. Jack, *Eur. Phys. J. B* **93**, 74 (2020).  
 [32] J. P. Garrahan, R. L. Jack, V. Lecomte, E. Pitard, K. van Duijvendijk, and F. van Wijland, *Phys. Rev. Lett.* **98**, 195702 (2007).  
 [33] V. Lecomte, C. Appert-Rolland, and F. van Wijland, *J. Stat. Phys.* **127**, 51 (2007).  
 [34] J. P. Garrahan, R. L. Jack, V. Lecomte, E. Pitard, K. van Duijvendijk, and F. van Wijland, *J. Phys. A* **42**, 075007 (2009).  
 [35] C. Maes, *Phys. Rep.* **850**, 1 (2020).  
 [36] F. Verstraete, M. M. Wolf, D. Perez-Garcia, and J. I. Cirac, *Phys. Rev. Lett.* **96**, 220601 (2006).  
 [37] F. Verstraete, V. Murg, and J. Cirac, *Adv. Phys.* **57**, 143 (2008).  
 [38] M. Lubasch, J. I. Cirac, and M.-C. Bañuls, *New J. Phys.* **16**, 033014 (2014).  
 [39] This is the case when we use the so-called “reduced tensor” scheme, but otherwise scales as  $O(D_{\text{PEPS}}^6)$ .  
 [40] K. Hyatt and E. M. Stoudenmire, (2019), [1908.08833](https://arxiv.org/abs/1908.08833).  
 [41] T. Vieijra, J. Haegeman, F. Verstraete, and L. Vanderstraeten, *Phys. Rev. B* **104**, 235141 (2021).  
 [42] M. Lubasch, J. I. Cirac, and M.-C. Bañuls, *Phys. Rev. B* **90**, 064425 (2014).  
 [43] Both are used with a decreasing update time-step  $\delta t \in [10^{-1}, 10^{-3}]$ , and the SU uses a minimum truncation cut-off error  $10^{-12}$ . The SU is used to serve an initial guess for the FU.  
 [44] E. Stoudenmire and S. R. White, *Annu. Rev. Condens. Matter Phys.* **3**, 111 (2012).  
 [45] We “snake” the MPS across the 2D lattice diagonally, running the DMRG algorithm with a fixed bond dimension. The algorithm is allowed enough sweeps until complete convergence in energy. The bond dimension is then routinely doubled, and the DMRG algorithm is run again. After each convergence, we record the energy and local observables. We check for convergence in the MPS bond dimension. If convergence is met (differences in energy and observables are smaller than  $10^{-5}$ ), we terminate the algorithm. We find a maximal bond dimension of  $D_{\text{MPS}} = 1024$  is sufficient to meet these criteria.  
 [46] B. Derrida, *J. Stat. Mech.* **2007**, P07023 (2007).  
 [47] T. Bodineau and B. Derrida, *C. R. Acad. Sci.* **8**, 540 (2007).  
 [48] C. Appert-Rolland, B. Derrida, V. Lecomte, and F. van

- Wijland, *Phys. Rev. E* **78**, 021122 (2008).
- [49] V. Lecomte, J. P. Garrahan, and F. van Wijland, *J. Phys. A* **45**, 175001 (2012).
- [50] R. L. Jack, I. R. Thompson, and P. Sollich, *Phys. Rev. Lett.* **114**, 060601 (2015).
- [51] T. Nemoto, R. L. Jack, and V. Lecomte, *Phys. Rev. Lett.* **118**, 115702 (2017).
- [52] D. Karevski and G. M. Schütz, *Phys. Rev. Lett.* **118**, 30601 (2017).
- [53] V. S. Borkar, S. Juneja, and A. A. Kherani, *Commun. Inf. Syst.* **3**, 259 (2003).
- [54] D. Simon, *J. Stat. Mech.: Theory Exp* **2009**, P07017 (2009).
- [55] R. L. Jack and P. Sollich, *Prog. Theor. Phys. Supp.* **184**, 304 (2010).
- [56] R. Chetrite and H. Touchette, *Ann. Henri Poincaré* **16**, 2005 (2015).
- [57] J. P. Garrahan, *J. Stat. Mech.: Theory Exp* **2016**, 073208 (2016).
- [58] L. Causer, M. C. Bañuls, and J. P. Garrahan, *Phys. Rev. E* **103**, 062144 (2021).
- [59] K. Ueda, R. Otani, Y. Nishio, A. Gendiar, and T. Nishino, *Journal of the Physical Society of Japan* **74**, 111 (2005), <https://doi.org/10.1143/JPSJS.74S.111>.
- [60] M. Frías-Pérez, M. Mariën, D. Pérez-García, M. C. Bañuls, and S. Iblisdir, (2021), [arXiv:2104.13264](https://arxiv.org/abs/2104.13264).
- [61] M. M. Rams, M. Mohseni, D. Eppens, K. Jałowiecki, and B. Gardas, *Phys. Rev. E* **104**, 025308 (2021).
- [62] L. Causer, M. C. Bañuls, and J. P. Garrahan, “Data for ‘optimal sampling of dynamical large deviations in two dimensions via tensor networks’,” (2022).
- [63] J. P. Garrahan and F. Pollmann, (2022), [arXiv:2203.08200](https://arxiv.org/abs/2203.08200).
- [64] P. G. Bolhuis, D. Chandler, C. Dellago, and P. L. Geissler, *Ann. Rev. Phys. Chem* **53**, 291 (2002).
- [65] Y. Tang, J. Liu, J. Zhang, and P. Zhang, (2022), [arXiv:2208.08266](https://arxiv.org/abs/2208.08266).